Vibrational and elastic properties of As4O6 and As4O6·2He at high pressures: Study of dynamical and mechanical stability

V. P. Cuenca-Gotor, O. Gomis, J. A. Sans, F. J. Manjón, P. Rodríguez-Hernández, and A. Muñoz

Citation: Journal of Applied Physics **120**, 155901 (2016); doi: 10.1063/1.4964875
View online: http://dx.doi.org/10.1063/1.4964875
View Table of Contents: http://scitation.aip.org/content/aip/journal/jap/120/15?ver=pdfcov
Published by the AIP Publishing

Vibrational and elastic properties of As_4O_6 and As_4O_6·2He at high pressures: Study of dynamical and mechanical stability

V. P. Cuenca-Gotor,[1] O. Gomis,[2,a)] J. A. Sans,[1] F. J. Manjón,[1] P. Rodríguez-Hernández,[3] and A. Muñoz[3]

[1]*Instituto de Diseño para la Fabricación y Producción Automatizada, MALTA Consolider Team, Universitat Politècnica de València, 46022 València, Spain*
[2]*Centro de Tecnologías Físicas: Acústica, Materiales y Astrofísica, MALTA Consolider Team, Universitat Politècnica de València, 46022 València, Spain*
[3]*Departamento de Física, Instituto de Materiales y Nanotecnología, MALTA Consolider Team, Universidad de La Laguna, 38205 Tenerife, Spain*

(Received 25 August 2016; accepted 4 October 2016; published online 18 October 2016)

The formation of a new compound with stoichiometry As_4O_6·2He at relatively low pressure (3 GPa) has been recently reported when arsenolite (As_4O_6) powder is compressed with helium as a pressure-transmitting medium. In this work, we study the lattice dynamics of As_4O_6 and As_4O_6·2He at high pressures from an experimental and theoretical perspective by means of Raman scattering measurements and *ab initio* calculations and report the theoretical elastic properties of both compounds at high pressure. Raman scattering measurements show a completely different behaviour of As_4O_6 and As_4O_6·2He at high pressures. Furthermore, the theoretical calculation of phonon dispersion curves and elastic stiffness coefficients at high pressure in both compounds allow us to discuss their dynamical and mechanical stability under hydrostatic compression. Both compounds are dynamically stable even above 35 GPa, but As_4O_6 becomes mechanically unstable at pressures beyond 19.7 GPa. These results allow explaining the pressure-induced amorphization of As_4O_6 found experimentally above 15–20 GPa and the lack of observation of any instability in As_4O_6·2He up to the highest studied pressure (30 GPa). *Published by AIP Publishing.*
[http://dx.doi.org/10.1063/1.4964875]

I. INTRODUCTION

Arsenic trioxide (As_2O_3) is a commercially important compound since it is the main precursor to other arsenic compounds, like organoarsenic compounds used in forestry products and pharmaceuticals. The oxide is also used in colorless glass production and in electronics as the precursor to elemental arsenic, arsenic alloys, and arsenide semiconductors.[1] Despite the well known toxicity of arsenic, arsenic trioxide has long been of biomedical interest, dating to traditional Chinese medicine, and is still used to treat cancer and other diseases.[2,3]

Arsenolite (α-As_2O_3, indeed As_4O_6) is a mineral which is formed by oxidation of As-rich ore deposits as arsenic sulfide or by hydrolysis of arsenic chloride.[4] This mineral constitutes the cubic polymorph [space group 227, *Fd*-3*m*, Z = 16] of arsenic oxide and is a molecular 3D solid with an open framework structure composed of closed-compact adamantane-type As_4O_6 molecular cages (with strong covalent interatomic As-O bonds) bonded together by weak van der Waals forces and directional intermolecular interactions[5,6] [see Fig. 1(a)]. In particular, the structure of the As_4O_6 molecular cage can be described by the overlap of four pseudo–tetrahedral units consisting of an As atom surrounded by three O ligands and a cationic lone electron pair (LEP) in such a way that they form a ball with all cation (also anion) LEPs pointing towards the external part of the cage.[7]

Apart from the structural characterization of As_4O_6 at high pressures (HPs),[8–10] the vibrational properties of arsenolite under compression have been also reported.[11,12] In Ref. 11, the pressure dependence of all (except one) Raman-active modes was reported as well as the pressure dependence of all infrared (IR)-active modes. Furthermore, additional modes were observed above 6 GPa, which were suggested to occur due to a cubic-to-tetragonal phase transition in As_4O_6. However, this phase transition has not been confirmed in the HP structural studies already performed.[8–10] Therefore, it is timely to revisit the vibrational properties of As_4O_6 at HP.

Several, previous works have reported the structural characterization of As_4O_6 under compression by means of angle dispersive x-ray diffraction (XRD) measurements using different pressure-transmitting media (PTMs).[8,10] In those works, it was shown that arsenolite is one of the most compressible non-hydrated minerals. Furthermore, it was shown that when this compound is compressed with He, this PTM enters into the largest voids of the structure (16d sites) above 3 GPa to form a stable compound with stoichiometry As_4O_6·2He [Fig. 1(b)].[8–10] In this regard, it is worth mentioning that it has been reported that As_4O_6 undergoes pressure-induced amorphization (PIA) above 15–20 GPa depending on the PTM used;[8,10–12] however, it was also shown that As_4O_6·2He remained stable at least up to 30 GPa showing no sign of PIA.[8–10]

a)Author to whom correspondence should be addressed. Electronic mail: osgohi@fis.upv.es

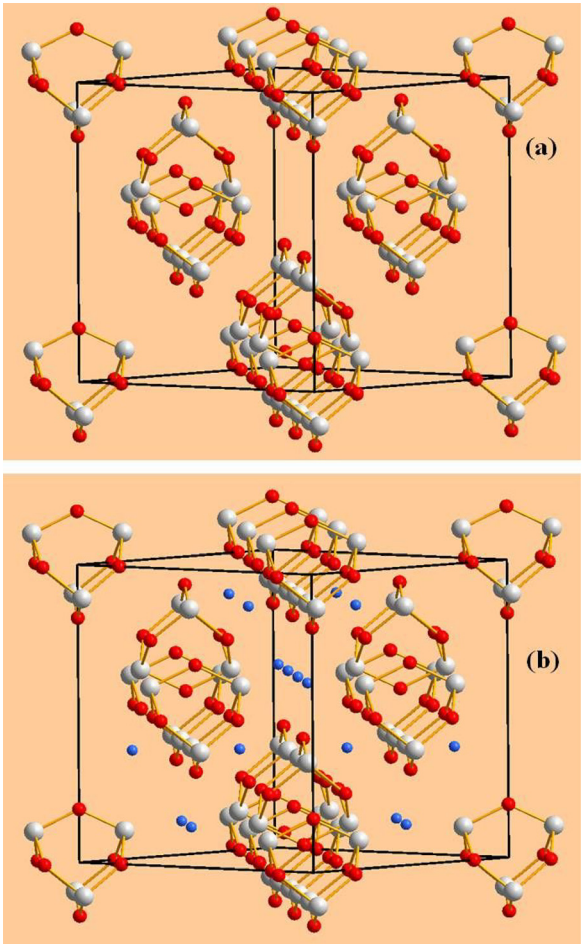

FIG. 1. Cubic unit cell of As_4O_6 (a) and $As_4O_6{\cdot}2He$ (b). Grey (big), red (medium), and blue (small) balls correspond to As, O, and He atoms, respectively.

In order to further understand the different behaviors of As_4O_6 and $As_4O_6{\cdot}2He$, we study in this work the lattice dynamics of both compounds by means of Raman scattering (RS) measurements at room temperature and *ab initio* calculations, as well as the theoretical elastic properties of both compounds at HP. Some thermodynamic properties are also reported in the supplementary material. In this way, we have theoretically studied the dynamical and mechanical stability of As_4O_6 and $As_4O_6{\cdot}2He$ at HP, which allows explaining prior experimental results. Note that partial results of the lattice dynamics and mechanical stability of both compounds were already reported in Refs. 8 and 10.

II. EXPERIMENTAL DETAILS

Highly pure arsenolite (As_4O_6) powder (99.999%) was commercially obtained from Sigma Aldrich Company. As_4O_6 powder was loaded inside a membrane-type diamond anvil cell (DAC) and was pressurized with different PTMs (4:1 methanol-ethanol mixture (MEM) and He) but also without any PTM. The ruby photoluminescence was used for pressure calibration in all measurements.[13]

HP-RS measurements at room temperature were performed in a backscattering geometry using a Horiba Jobin-Yvon LabRam HR UV spectrometer in combination with a thermoelectrically cooled multichannel CCD detector (resolution below 2 cm^{-1}). RS spectra of arsenolite powder were excited either with 532.0 or 632.8 nm laser lines and laser power below 10 mW up to pressures between 12 and 22 GPa. RS measurements were analyzed by fitting Raman peaks with a Voigt profile fixing the Gaussian line width to the experimental setup resolution.

III. THEORETICAL CALCULATIONS DETAILS

Ab initio total-energy calculations were performed within the density functional theory (DFT)[14] using the plane-wave method[15] and the pseudopotential theory with the Vienna *ab initio* simulation package (VASP)[16] as in a previous work.[10] Convergence tests show that in order to have accurate results, the plane wave basis requires an energy cutoff of 520 eV. The integrations in the Brillouin zone were performed using a special k-point sampling, with dense $(4 \times 4 \times 4)$ grid of k-points in order to have high accurate and converged results. Total energies were converged up to 0.001 eV/atom and forces acting on atoms were converged up to 0.003 eV/Å. The exchange and correlation term was computed through Perdew-Burke-Ernzerhof (PBE) for solids' prescription.[17] In this way, lattice dynamics *ab initio* calculations at the zone center (Γ point) of the Brillouin zone (BZ) were performed using the direct force constant approach.[18] To obtain the phonon dispersion curves (PDCs) along high-symmetry directions of the BZ, we performed similar calculations using appropriate supercells, which allow the phonon dispersion at k-points to be obtained commensurate with the supercell size.[18]

On the other hand, *ab initio* calculations allow the study of the mechanical properties of materials. In particular, the elastic constants describe the mechanical properties of materials in the region of small deformations where the stress-strain relations are still linear. The elastic constants can be obtained by computing the macroscopic stress for a small strain with the use of the stress theorem.[19] In the present work, we perform the evaluation of the elastic constants of As_4O_6 and $As_4O_6{\cdot}2He$ with the use of the DFT as implemented in VASP.[20] The ground state and fully relaxed structures were strained in different directions according to their symmetry.[20] The total-energy variations were evaluated according to a Taylor expansion for the total energy with respect to the applied strain.[21] Due to this fact, it is important to check that the strain used in the calculations guarantees the harmonic behavior. This procedure allows us to obtain the C_{ij} elastic constants in the Voigt notation. The number of independent elastic constants is reduced by crystalline symmetry.[22]

IV. RESULTS AND DISCUSSION

A. Lattice dynamics

Arsenolite has a primitive unit cell containing two As_4O_6 adamantanoid molecules situated on the T_d sites of the unit cell.[23] According to the factor group analysis, arsenolite, as well as senarmontite, has 60 vibrational modes at zone center:[24] $\Gamma = 2A_{1g} + 2A_{2u} + 2E_g + 2E_u + 3T_{1g} + 3T_{2u} + 5T_{2g} + 5T_{1u}$, where E and T modes are double and triple degenerated, respectively. In this way, there are nine Raman-

active modes: $2A_{1g} + 2E_g + 5T_{2g}$, four IR-active modes: $4T_{1u}$, ten inactive modes: $2A_{2u} + 2E_u + 3T_{1g} + 3T_{2u}$, and one acoustic mode: T_{1u}.[25] Most of the above optical modes come from the internal modes of the isolated As_4O_6 molecule: $\Gamma_{vib} = 2A_1 + 2E + 2T_1 + 4T_2$ due to crystal field (or Davydov) splitting.[26] From now on, we will add to the optical vibrational modes of a given symmetry a superscript in order of increasing frequency for the sake of clarity.

To date, several studies have been published on arsenolite's Raman spectra at room conditions[25–30] and only two at HP.[11,12] In the first works, there was some disagreement on the assignment of T_{2g} and E_g modes, which has been finally clarified;[26,30] however, there remains one E_g vibrational mode yet to be clearly observed and identified.[26,30] In the following, we will report the pressure dependence of the different Raman-active modes with different PTMs and will show the identification of the lost E_g mode.

1. As_4O_6 pressurized with MEM as a PTM

MEM is a good quasi-hydrostatic PTM up to 20 GPa which is not expected to enter into the open framework structure of arsenolite. Figure 2(a) shows the RS spectra of As_4O_6 compressed with MEM up to 21 GPa. As observed, our RS spectra are similar to those already reported.[11,12] Figure 2(b) shows the pressure dependence of the experimental and theoretical Raman-active modes of As_4O_6. Upon compression, several modes shift to upper wavenumbers: the $T_{2g}{}^1$ mode at 84 cm^{-1}; the $T_{2g}{}^2$ mode at 268 cm^{-1}; the $T_{2g}{}^3$ at 413 cm^{-1}; the $A_{1g}{}^2$ mode at 560 cm^{-1}; and the $T_{2g}{}^5$ mode at 780 cm^{-1}. On the other hand, there are a few modes which shift to lower wavenumbers: the $E_g{}^1$ mode at 183 cm^{-1}; the $A_{1g}{}^1$ mode at 369 cm^{-1}; and the $T_{2g}{}^4$ at 470 cm^{-1}. Due to the closeness of the $T_{2g}{}^3$ and $T_{2g}{}^4$ modes, these two modes undergo a phonon anticrossing around 4.5 GPa, i.e., these two modes repel each other at around 4.5 GPa, then the $T_{2g}{}^3$ band gains intensity and shifts to lower wavenumbers, while the $T_{2g}{}^4$ band loses intensity and shifts to upper wavenumbers. Our symmetry assignments performed on the basis of our theoretical calculations agree with those of Grzechnik and Gilliam *et al.*[11,30] Furthermore, our *ab initio* calculations indicate that there is an E_g mode at 420 cm^{-1}, which is the only Raman-active mode that was not clearly found in previous Raman works. Taking into account that our calculated frequencies underestimate the experimental frequencies, it is expected that the lost E_g mode could be the weak mode near 443 cm^{-1} observed as a shoulder of the intense $T_{2g}{}^4$ mode by Lockwood and Gilliam *et al.*[29,30] However, we have not observed this mode in RS measurements of As_4O_6 at room conditions or at HP using MEM as a PTM.

Apart from the first-order Raman-active modes, other modes are observed in the RS spectrum of arsenolite as noted by many authors. In particular, we have observed a very weak peak at about 80 cm^{-1} (also seen in Ref. 11) close to the $T_{2g}{}^1$ mode at 84 cm^{-1}. In our opinion, this extra mode can be tentatively assigned to one of the inactive librational modes, likely $T_{1g}{}^1$, of the As_4O_6 molecule due to the close similarity of the theoretical frequencies and pressure coefficients of this mode (see Fig. 2(b)), where the theoretical pressure dependence of the two lowest frequency inactive modes is also plotted. We think that this inactive mode could be observed due to local loss of translational periodic conditions in As_4O_6 as pressure increases. Furthermore, with increasing pressure, many Raman modes undergo a progressive asymmetric broadening resulting in split modes mainly above 10 GPa. These features, which were also noted in Ref. 11, are likely caused by the increase of intermolecular interactions, i.e., the increase of interactions among As_4O_6 cages, which finally results in the onset of PIA above 15–20 GPa depending on the PTM used. On the other hand, the reversibility of the changes in the RS spectra above 10 GPa shows little or no hysteresis. We must note that the increase of intermolecular interactions does not result in a reversible phase transition above 6 GPa as suggested by Grzechnik.[11]

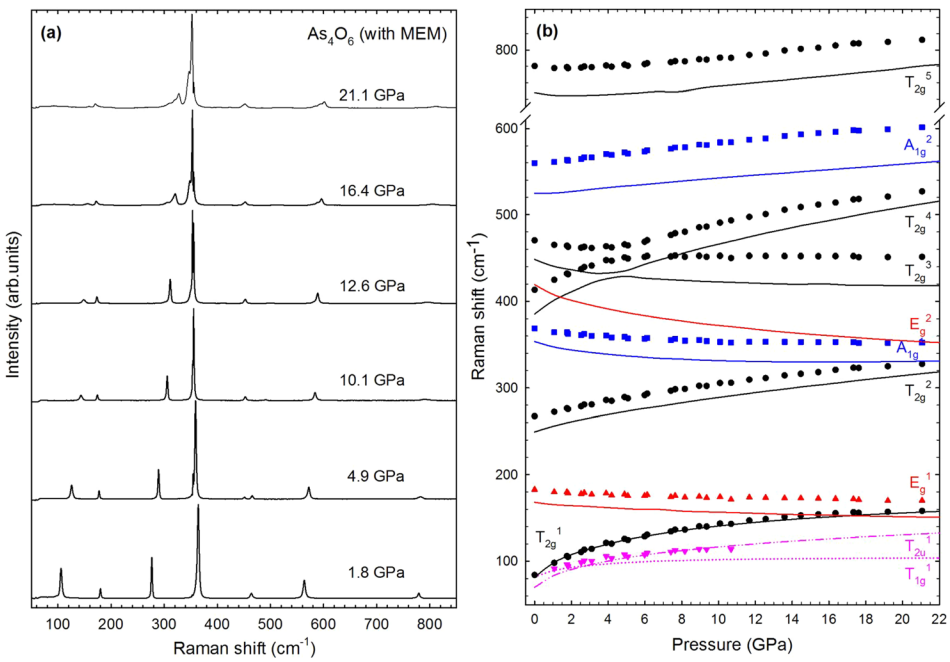

FIG. 2. (a) Raman spectra of As_4O_6 up to 21 GPa when pressurized with a 4:1 methanol-ethanol mixture. (b) Pressure dependence of the experimental (symbols) and theoretical (solid lines) Raman-mode frequencies. The theoretical $T_{1g}{}^1$ ($T_{2u}{}^1$) inactive mode is shown with a dotted (dashed-dotted) line. Pink symbols represent the extra Raman modes observed or used to fit the profile of broadened asymmetric peaks on increasing pressure.

TABLE I. Experimental and theoretical frequencies and pressure coefficients of Raman-active (R) modes in As_4O_6 at 0 GPa. The inactive modes T_{2u}^{1} and T_{1g}^{1} are also included.

	Ab initio calculations		Experiments					
Mode (Sym)	ω_0 (cm^{-1})	$\frac{\partial\omega}{\partial P}\left(\frac{cm^{-1}}{GPa}\right)$	ω_0^a (cm^{-1})	$\frac{\partial\omega^a}{\partial P}\left(\frac{cm^{-1}}{GPa}\right)$	ω_0^b (cm^{-1})	$\frac{\partial\omega^b}{\partial P}\left(\frac{cm^{-1}}{GPa}\right)$	ω_0^c (cm^{-1})	$\frac{\partial\omega^c}{\partial P}\left(\frac{cm^{-1}}{GPa}\right)$
T_{2u}^{1}	70.7	11.9						
T_{1g}^{1}	81.8	7.8	85.5	6.0	82.3	8.9		
T_{2g}^{1} (R)	82.1	15.2	84.7	12.9	83.8	13.2	81.0	10.0
E_g^{1} (R)	168.0	−2.5	182.5	−2.3	182.6	−2.0	181.1	−1.0
T_{2g}^{2} (R)	249.4	6.4	267.5	4.9	267.1	5.0	265.2	3.9
A_{1g}^{1} (R)	353.4	−5.7	368.6	−3.6	368.7	−3.0	367.2	−2.0
T_{2g}^{3} (R)	385.4	16.0	413.4	11.8	413.2	11.6	410.6	10.0
E_g^{2} (R)	418.9	−10.4			449.2	−6.4		
T_{2g}^{4} (R)	448.5	−8.7	470.3	−5.6	470.5	−5.1	469.8	−3.0
A_{1g}^{2} (R)	524.6	0.5	559.4	1.7	559.3	2.0	558.8	1.4
T_{2g}^{5} (R)	747.9	−3.7	780.0	−1.5	780.5	−2.3	780.5	−0.6

[a]Experiment with MEM.
[b]Experiment without any PTM.
[c]Experiment with CsI (data from Ref. 11).

Previous XRD measurements confirmed that the cubic symmetry is maintained up to the onset of PIA.[8–10] Table I summarizes the experimental and theoretical zero-pressure frequencies, pressure coefficients, and derivative of the pressure coefficients for the Raman-active modes of arsenolite. As observed, our results for the Raman-active modes at zero pressure compare well with the previous results reported by Grzechnik[11] and also with those of Gilliam *et al.*[30] at ambient pressure.

For completeness, we have compared the theoretical pressure dependence of the IR-active modes of As_4O_6 with the experimental data taken from Ref. 11 (see Fig. S1 in the supplementary material). As observed, there is a rather good agreement between the experimental and theoretical data, so our calculations confirm the four IR-active modes already reported for arsenolite.[11,28] The experimental and theoretical zero-pressure frequencies, pressure coefficients, and derivative of the pressure coefficients for the IR-active modes of arsenolite are given in Table SI of the supplementary material.

2. As_4O_6 pressurized without any PTM

For a better comparison of our HP-RS measurements on As_4O_6 with those of Ref. 11, which were performed with CsI as a PTM, and with those of Ref. 12, which were performed without any PTM, we performed measurements without any PTM since arsenolite is a rather good quasi-hydrostatic PTM at low pressures (in fact slightly better than CsI).[31] RS spectra of As_4O_6 without PTM were measured up to 12 GPa (Fig. S2 in the supplementary material). A detail of the Raman spectra in the region between 400 and 500 cm^{-1}, where the E_g mode is expected to be observed, is plotted in Fig. 3(a) and the

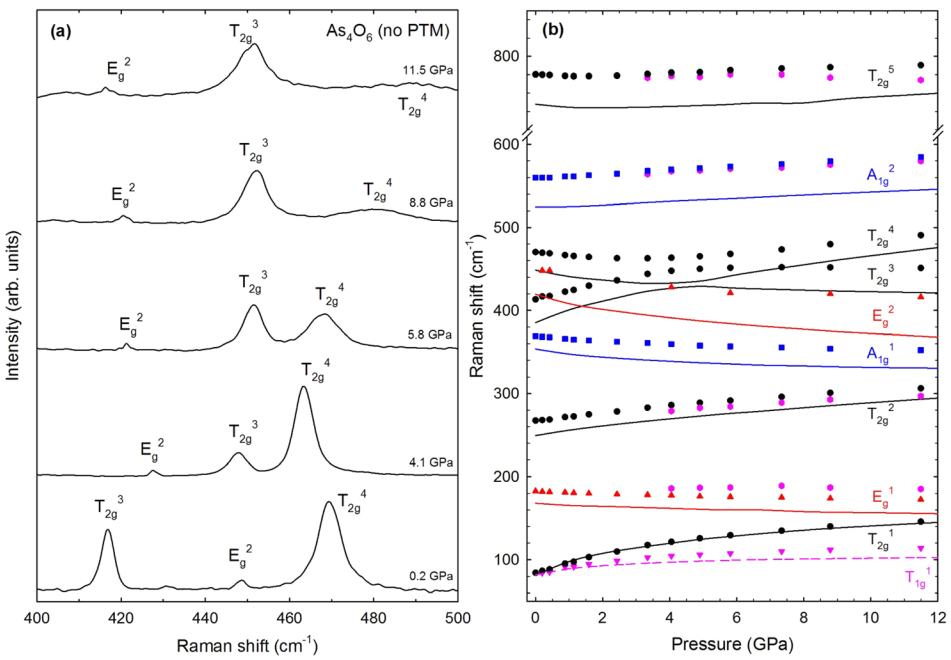

FIG. 3. (a) Detail of the Raman spectra of As_4O_6 up to 12 GPa when pressurized without any pressure-transmitting medium. (b) Pressure dependence of the experimental (symbols) and theoretical (solid lines) Raman-mode frequencies. The theoretical T_{1g}^{1} inactive mode is shown with a dashed line. Pink symbols represent the extra Raman modes observed or used to fit the profile of asymmetric peaks.

pressure dependence of the frequencies of its Raman-active modes is reported (Fig. 3(b)). The frequencies and pressure coefficients of the Raman-active modes in As_4O_6 pressurized without any PTM are also shown in Table I.

Raman-active modes of As_4O_6 pressurized without any PTM show a similar behaviour with increasing pressure as in the case of As_4O_6 pressurized with MEM. However, the width of the Raman-active modes increases with pressure at a much faster rate, i.e., at smaller pressures, than using MEM. Curiously, we have found a weak mode near 448 cm^{-1} at room pressure whose pressure dependence is consistent with the theoretical evolution of the E_g^2 mode (see Figs. 3(a) and 3(b) and Table I). Therefore, we have tentatively attributed this weak mode to the lost E_g^2 mode. We have to note that this means that there are three Raman-active modes in the RS of arsenolite in the region from 400 to 500 cm^{-1}. In this respect, previous RS measurements of arsenolite compressed without any PTM already reported three Raman active modes in this region in the RS spectrum at 11 GPa.[12] However, this work does not report any analysis of the experimental Raman-active mode frequencies of arsenolite as a function of pressure. We have also to note that the frequency we have found is slightly larger than the one reported by Gilliam *et al.*,[30] but in very good agreement with Hartree-Fock calculations of Jensen *et al.*[26] At present, we do not know why it has been easier to find this mode under quasi-hydrostatic conditions than under truly hydrostatic conditions (this mode was also not observed when pressurizing with He). We can speculate that the small RS cross section already known for this mode[26] can be enhanced by altering selection rules under non-hydrostatic conditions.

3. As_4O_6 pressurized with helium as a PTM

Helium provides the most hydrostatic conditions for HP experiments, but He is so a small atom that it can enter into the cavities of open framework structures present in porous and molecular materials. We have performed a study of As_4O_6 pressurized with He in order to study the effect of He into the compression of this molecular solid. In this regard, we showed in a previous work that He enters into the 16d sites of As_4O_6 and reacts with this molecular solid forming a new compound with stoichiometry $As_4O_6{\cdot}2He$ above 3 GPa.[10]

$As_4O_6{\cdot}2He$ has the same cubic structure as As_4O_6 with two formula units per primitive cell. Therefore, according to group theory, $As_4O_6{\cdot}2He$ has 62 vibrational modes at zone center:[24] $\Gamma = 2A_{1g} + 2A_{2u} + 2E_g + 2E_u + 3T_{1g} + 3T_{2u} + 5T_{2g} + 7T_{1u}$. In this way, there are nine Raman-active modes: $2A_{1g} + 2E_g + 5T_{2g}$, six IR-active modes: $6T_{1u}$, ten inactive modes: $2A_{2u} + 2E_u + 3T_{1g} + 3T_{2u}$, and one (triply degenerated) acoustic mode: T_{1u}. In summary, there are only two additional IR-active modes in $As_4O_6{\cdot}2He$ than in As_4O_6.

Figure 4(a) shows the pressure dependence of the RS spectra of As_4O_6 compressed with He up to 3 GPa and of $As_4O_6{\cdot}2He$ from 3 GPa up to 12 GPa. The experimental and theoretical pressure dependence of the different Raman-active modes is presented in Fig. 4(b). The frequencies and pressure coefficients of the Raman-active modes in $As_4O_6{\cdot}2He$ are shown in Table II. As observed, the pressure dependence of Raman-active modes up to 2 GPa follows the same behaviour as As_4O_6 modes studied in Sections IV A 1 and IV A 2. However, between 2 and 3 GPa, many Raman modes undergo a sudden change in frequency. No further sudden change in frequencies is observed above 3 GPa and RS modes from 3 GPa on behave in a different way to Raman-active modes of As_4O_6. Noteworthy, the anti-crossing between the two T_{2g} modes, which occurs in As_4O_6 around 4.5 GPa, is retarded up to 11 GPa in $As_4O_6{\cdot}2He$. The good agreement of our experimental and theoretical data in this regard is a clear confirmation of the entrance of He into 16d sites of the arsenolite structure. Since we have not performed IR measurements in $As_4O_6{\cdot}2He$, the pressure dependence of the theoretically IR-active modes of $As_4O_6{\cdot}2He$ is

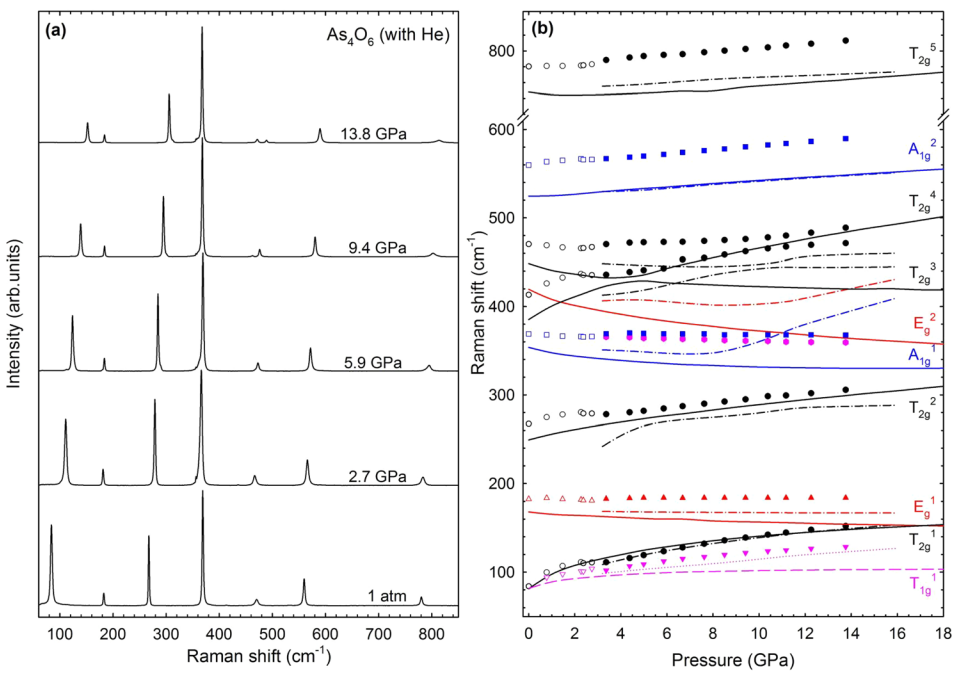

FIG. 4. (a) Raman spectra of As_4O_6 up to 3 GPa and of $As_4O_6{\cdot}2He$ from 3 GPa up to 14 GPa. (b) Pressure dependence of the experimental (full symbols) and theoretical (dashed-dotted lines) Raman-mode frequencies of $As_4O_6{\cdot}2He$. Experimental Raman-mode frequencies for As_4O_6 up to 3 GPa are shown with empty symbols. Theoretical data for As_4O_6 (solid lines) are also shown for comparison with those of $As_4O_6{\cdot}2He$ to note the effect of He entrance in 16d sites of As_4O_6. The theoretical T_{1g}^1 inactive mode is shown in pink with a dashed line for As_4O_6 and with a dotted line for $As_4O_6{\cdot}2He$. Pink symbols represent the extra Raman modes observed or used to fit the profile of asymmetric peaks.

TABLE II. Experimental and theoretical frequencies and pressure coefficients of Raman-active (R) modes in $As_4O_6{\cdot}2He$ at 3 GPa. The inactive mode $T_{1g}{}^1$ is also included.

	Ab initio calculations		Experiments	
Mode (Sym)	ω_0 (cm^{-1})	$\frac{\partial\omega}{\partial P}\left(\frac{cm^{-1}}{GPa}\right)$	ω_0 (cm^{-1})	$\frac{\partial\omega}{\partial P}\left(\frac{cm^{-1}}{GPa}\right)$
$T_{1g}{}^1$	98.9	2.3	102.0	3.6
$T_{2g}{}^1$ (R)	108.2	6.6	108.8	6.7
$E_g{}^1$ (R)	168.7	−0.3	183.1	0.4
$T_{2g}{}^2$ (R)	244.3	10.0	276.4	3.3
$A_{1g}{}^1$ (R)	349.7	−4.9	369.8	−0.3
$T_{2g}{}^3$ (R)	412.3	−0.7	435.0	−1.3
$E_g{}^2$ (R)	409.2	−5.9		
$T_{2g}{}^4$ (R)	448.7	−2.4	469.7	3.7
$A_{1g}{}^2$ (R)	528.8	1.8	565.7	2.2
$T_{2g}{}^5$ (R)	754.7	2.2	788.6	2.0

reported in Fig. S3 in the supplementary material for comparison with future experimental works. As observed, there are two extra IR-active modes in $As_4O_6{\cdot}2He$ between 200 and 300 cm^{-1} whose pressure coefficient is much larger than those coming from As_4O_6.

B. Dynamical stability

To finish the study of the lattice dynamics of As_4O_6 and $As_4O_6{\cdot}2He$ at HP, we report the calculation of PDCs for both compounds at selected pressures which allows the discussion of their dynamical stability under hydrostatic compression.[32] Figure 5 shows the PDCs of As_4O_6 at 0 GPa and 34.7 GPa, while Fig. 6 shows the PDCs of $As_4O_6{\cdot}2He$ at 5.2 GPa and 35.5 GPa. It can be observed that there is no phonon dispersion relation that undergoes softening to zero frequency on increasing pressure neither in As_4O_6 up to 34.7 GPa nor in $As_4O_6{\cdot}2He$ up to 35.5 GPa. Therefore, we safely conclude that the cubic structure of both compounds is dynamically stable at least up to those pressures.

C. Elastic properties

Since the cubic structures of As_4O_6 and $As_4O_6{\cdot}2He$ belong to the Fd-3m space group, they have point group 4/m–3 2/m, also known as m-3m (or O_h), and belong to the cubic Laue group m-3m (or C I)[33] which has three independent second order elastic constants: C_{11}, C_{12}, and C_{44}. When a non-zero uniform stress is applied to the crystal, the elastic properties are described by the elastic stiffness (or stress-strain) coefficients, which are defined as

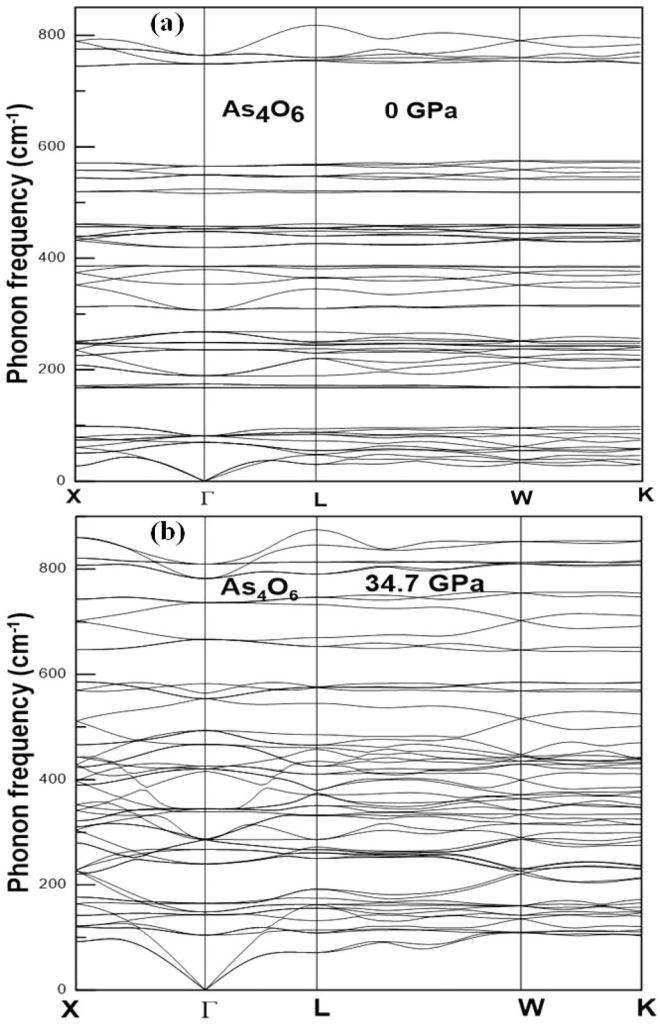

FIG. 5. Phonon dispersion curves of As_4O_6 at 0 GPa (a) and 34.7 GPa (b).

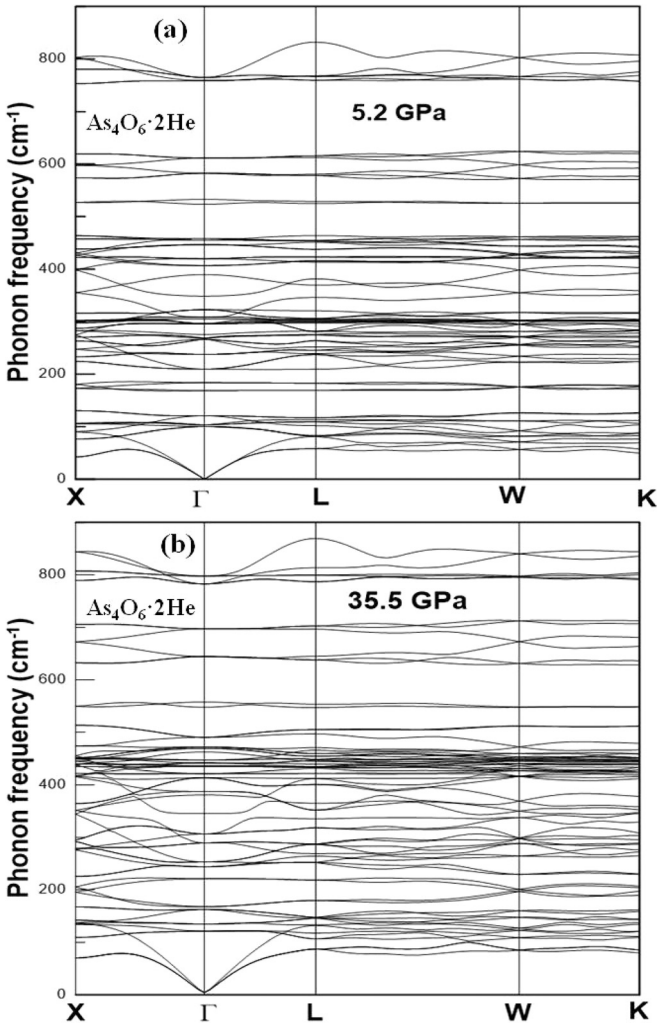

FIG. 6. Phonon dispersion curves of $As_4O_6{\cdot}2He$ at 5.2 GPa (a) and 35.5 GPa (b).

TABLE III. C_{ij} elastic constants (in GPa) for As_4O_6 and $As_4O_6{\cdot}2He$ at 0 GPa. Elastic moduli B_H, G_H, and E_H (in GPa), and Possion's ratio (ν_H) given in the Hill approximation, labeled with subscript H in As_4O_6 and $As_4O_6{\cdot}2He$ at 0 GPa. The B_H/G_H ratio, Zener anisotropy factor (A), Vickers hardness (H_v in GPa), density (ρ in g/cm^3), and longitudinal (v_{lon}), transverse (v_{trans}), and averaged (v_m) elastic wave velocities (all in m/s) are also included.

	As_4O_6	$As_4O_6{\cdot}2He$
C_{11}	21.2	28.8
C_{12}	4.0	−0.6
C_{44}	9.8	8.7
B_H	9.8	9.2
G_H	9.3	10.7
E_H	21.2	23.1
ν_H	0.14	0.08
B_H/G_H	1.05	0.86
A	1.15	0.59
H_v	4.2	5.8
P	3.982	3.766
v_{lon}	2359.8	2495.3
v_{trans}	1529.6	1684.1
v_m	1678.0	1838.1

$$B_{ijkl} = C_{ijkl} + 1/2\,[\delta_{ik}\sigma_{jl} + \delta_{jk}\sigma_{il} + \delta_{il}\sigma_{jk} + \delta_{jl}\sigma_{ik} - 2\delta_{kl}\sigma_{ij}], \quad (1)$$

with C_{ijkl} being the elastic constants evaluated at the current stressed state, σ_{ij} correspond to the external stresses, and δ_{kl} is the Kronecker delta.[34–36] In the special case of hydrostatic pressure ($\sigma_{11} = \sigma_{22} = \sigma_{33} = -P$) applied to a cubic crystal, the elastic stiffness coefficients in the Voigt notation B_{ij} are: $B_{11} = C_{11} - P$, $B_{12} = C_{12} + P$, and $B_{44} = C_{44} - P$, where P is the hydrostatic pressure. Note that the B_{ij} and C_{ij} are equal at 0 GPa. When the elastic stiffness coefficients B_{ij} are used, all relationships of the elasticity theory can be applied for the crystal under any loading, including Born's stability conditions which are identical in both loaded and unloaded states.[35–39] Table III summarizes the values of the three elastic constants C_{ij} in As_4O_6 and $As_4O_6{\cdot}2He$ at 0 GPa as obtained from our *ab initio* calculations. As observed, C_{11} is larger in $As_4O_6{\cdot}2He$ than in As_4O_6, while C_{12} and C_{44} are smaller in $As_4O_6{\cdot}2He$ than in As_4O_6.

Figure 7 shows the pressure dependence of the elastic constants, C_{ij}, and elastic stiffness coefficients, B_{ij}, in As_4O_6 and $As_4O_6{\cdot}2He$. Despite only B_{ij} are meaningful at any pressure, we report also the pressure dependence of C_{ij} because they are the original magnitudes computed from which B_{ij} are obtained. As observed, C_{11} (and B_{11}) has a larger pressure coefficient in $As_4O_6{\cdot}2He$ than in As_4O_6, while C_{12} (and B_{12}) and C_{44} (and B_{44}) have smaller pressure coefficients in $As_4O_6{\cdot}2He$ than in As_4O_6. Besides, C_{11} (and B_{11}) and C_{12} (and B_{12}) increase with increasing pressure both in As_4O_6 and $As_4O_6{\cdot}2He$, while C_{44} (and B_{44}) tends to saturate with increasing pressure in As_4O_6 but not in $As_4O_6{\cdot}2He$. These results will be discussed later in relation with the mechanical stability of both compounds.

Standard analytical formulas for the bulk (B) and shear (G) moduli in the Voigt,[40] Reuss,[41] and Hill[42] approximations, labeled with subscripts V, R, and H, respectively, can be obtained from the set of B_{ij} for any loading in As_4O_6 and $As_4O_6{\cdot}2He$[43]

$$B_V = B_R = \frac{B_{11} + 2B_{12}}{3}, \quad (2)$$

$$B_H = \frac{B_V + B_R}{2}, \quad (3)$$

$$G_V = \frac{B_{11} - B_{12} + 3B_{44}}{5}, \quad (4)$$

$$G_R = \frac{5(B_{11} - B_{12})B_{44}}{4B_{44} + 3(B_{11} - B_{12})}, \quad (5)$$

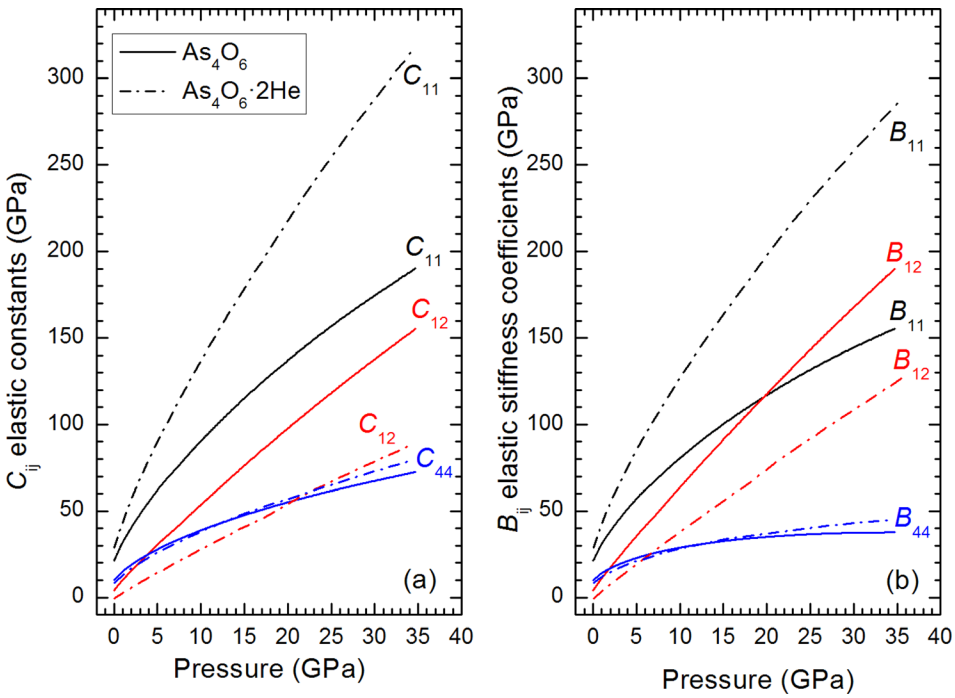

FIG. 7. Pressure dependence of the theoretical elastic constants (a) and elastic stiffness coefficients (b) in As_4O_6 and $As_4O_6{\cdot}2He$.

$$G_H = \frac{G_V + G_R}{2}. \quad (6)$$

In the Voigt (Reuss) approximation, uniform strain (stress) is assumed throughout the polycrystal.[40,41] Hill has shown that the Voigt and Reuss averages are limits and suggested that the actual effective B and G elastic moduli can be approximated by the arithmetic mean of the two bounds.[42] The Young (E) modulus and the Poisson's ratio (ν) are calculated with the expressions[44,45]

$$E_X = \frac{9B_X G_X}{G_X + 3B_X}, \quad (7)$$

$$\nu_X = \frac{1}{2}\left(\frac{3B_X - 2G_X}{3B_X + G_X}\right), \quad (8)$$

where the subscript X refers to the symbols V, R, and H. In this work, we report the elastic moduli in the Hill approximation. We summarize in Table III all the values obtained for B_H, G_H, and E_H in As_4O_6 and As_4O_6·2He at 0 GPa. Note that our calculated value for the bulk modulus in the Hill approximation is 9.8 (9.2) GPa for As_4O_6 (As_4O_6·2He), which is in rather good agreement with the value of $B_0 = 7.6$ (6.4) GPa obtained from our PBEsol structural calculations via a fit to a third-order Birch Murnaghan equation of state[8,10] and with those of Birch-Murnaghan EoS fit to p(V) data computed within the PAW_PBE-D2 approach in Ref. 9. Furthermore, both values are comparable to experimental values of $B_0 = 7(2)$ GPa and 4(2) GPa obtained via a fit to a third-order Birch Murnaghan equation of state for As_4O_6 and As_4O_6·2He, respectively.[8,10] Note that the bulk modulus of As_4O_6·2He at zero pressure was extrapolated from the data above 3 GPa since this compound is not stable below this pressure.

The above results give us confidence about the correctness of our elastic constants calculations. With this subject in mind, we have compared the bulk modulus and shear modulus in both compounds, which is indicative of the difference between the elastic behavior of both compounds. In As_4O_6, the bulk modulus is larger than the shear modulus, while in As_4O_6·2He the contrary is observed. This means that As_4O_6 is more resistive to compression than to shear stresses, while the contrary is observed in As_4O_6·2He.

Table III also includes the values of the Poisson's ratio, ν_H, the ratio between the bulk and shear modulus, B_H/G_H, and the Zener elastic anisotropy factor, A, at 0 GPa for both compounds. The Poisson's ratio provides information about the characteristics of the bonding forces and chemical bonding. The value of the Poisson's ratio in the Hill approximation is $\nu = 0.14$ (0.08) in As_4O_6 (As_4O_6·2He). This value indicates that the interatomic bonding forces are predominantly noncentral ($\nu < 0.25$) and that directional intramolecular and intermolecular bonding is predominant at 0 GPa.[5,46,47]

The B_H/G_H ratio is a simple relationship given by Pugh,[48] empirically linking the plastic properties of a material with its elastic moduli. According to the Pugh criterion, a high B_H/G_H ratio is associated with ductility, whereas a low ratio corresponds to brittleness. The critical value for the B_H/G_H ratio is around 1.75, which separates ductile and brittle materials. In our study, we have found values of B/G at 0 GPa below 1.75 for As_4O_6 and As_4O_6·2He. Therefore, both compounds are fragile at zero pressure, being As_4O_6·2He more fragile than As_4O_6.

One of the elastic properties of crystals with more importance for both engineering science and crystal physics is the elastic anisotropy, because it is highly correlated with the possibility of inducing microcracks in materials.[49] This anisotropy can be quantified with the Zener anisotropy factor which is defined as $A = 2B_{44}/(B_{11}-B_{12})$. If A is equal to 1, no anisotropy exists. On the other hand, the more this parameter differs from 1 the more elastically anisotropic is the crystalline structure. The value of A for As_4O_6 is closer to 1 than for the case of As_4O_6·2He. Therefore, the latter is more elastically anisotropic than the former at 0 GPa.

Figures 8 and 9 show the pressure dependence of B, G, and E elastic moduli, ν, B/G ratio, and A, in As_4O_6 and As_4O_6·2He. It can be noted that B_H, increases with pressure reaching a maximum value close to 115 GPa in both compounds at 20 GPa. Contrarily, G_H and E_H increase with pressure up to 9 GPa in As_4O_6 and decrease for larger pressures. This behavior is different to that of As_4O_6·2He where both G_H and E_H increase with pressure up to the maximum calculated pressure (35.5 GPa).

On the other hand, the Poisson's ratio shows a curious pressure dependence in both compounds. It strongly increases with pressure up to 2 GPa and then tends to saturate above this pressure. It reaches a value of 0.46 (0.32) at 20 GPa for As_4O_6 (As_4O_6·2He). These values indicate an increment of the ductility and of the metallic behavior, i.e., the progressive loss of interatomic bond directionality, with increasing pressure in both compounds. It must be stressed that the approximation of the Poisson's ratio in As_4O_6 to 0.5 (superior limit of the Poisson's ratio) near 20 GPa is likely due to the tendency of As_4O_6 towards a mechanical instability.[47] Note that the B/G ratio, which is related to the Poisson's ratio,[47] also increases with pressure in the two compounds; however, the increase is

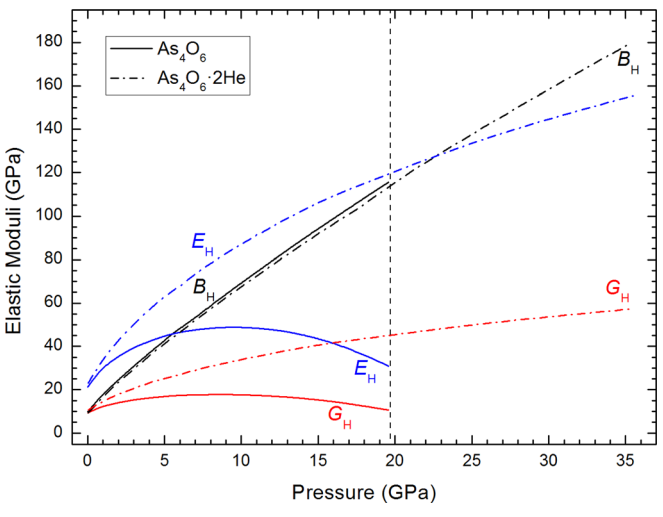

FIG. 8. Pressure dependence of the elastic moduli B_H, G_H, and E_H in As_4O_6 and As_4O_6·2He.

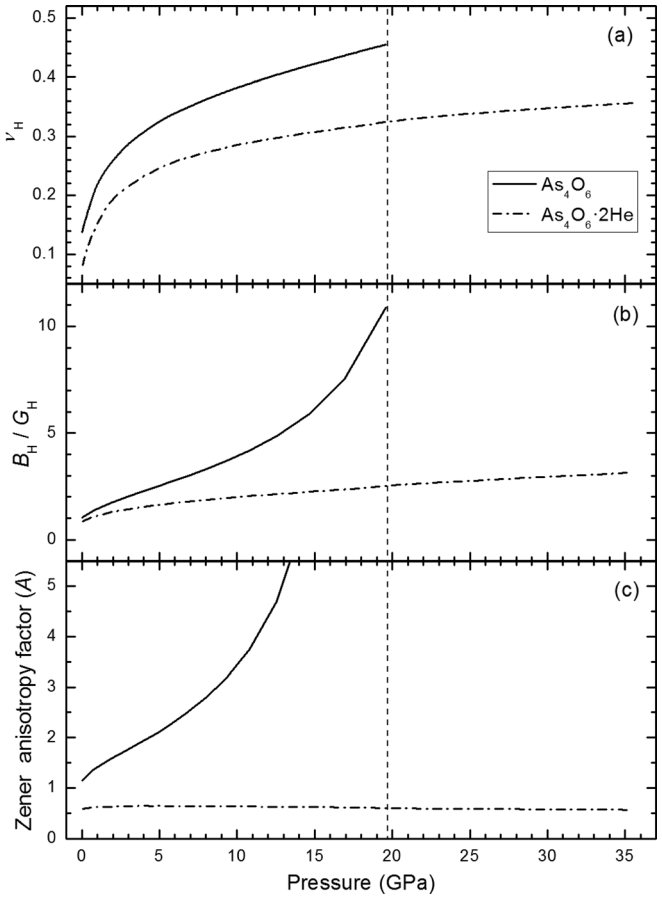

FIG. 9. Pressure dependence of the Poisson's ratio (ν_H), B_H/G_H ratio, and Zener anisotropy factor (A) in As_4O_6 and As_4O_6·2He.

moderate in As_4O_6·2He and abrupt in As_4O_6 above 10 GPa, thus suggesting the presence of a mechanical instability in this later compound. Finally, the Zener anisotropy factor also shows a quite different behavior in both compounds. It increases considerably in As_4O_6 especially above 10 GPa, while it stays nearly constant (around 0.6) in As_4O_6·2He. Again, these results indicate that the elastic anisotropy strongly increases in As_4O_6 with pressure, but it remains constant in As_4O_6·2He. Therefore, the strong increase of the elastic anisotropy in As_4O_6 with pressure could be also understood as a signal of a mechanical instability in arsenolite at high pressure.

One of the most common elastic properties and less easy to handle is hardness, which is a property generally related to both the elastic and plastic properties of a material. Hardness is an unusual physical property because it is not an intrinsic materials property, but the result of a defined measurement procedure susceptible to precise definitions in terms of fundamental units of mass, length, and time. In practice, hardness is measured by the size of the indentation made on a specimen by a load of a specified shape when a force is applied during a certain time. In this way, there are three principal standard methods for expressing the relationship between the hardness and the size of the indentation, these being Brinell, Rockwell, and Vickers. The Vickers hardness, H_v, can be calculated by the formula proposed by Tian *et al.*[50]

$$H_v = 0.92(G/B)^{1.137}G^{0.708}. \quad (9)$$

We used this formula as it eliminates the possibility of unrealistic negative hardness. The values of H_v for As_4O_6 and As_4O_6·2He at 0 GPa are included in Table III. As observed, As_4O_6·2He is harder than As_4O_6 and both have values of H_v that are approximately between 4 and 6 GPa at 0 GPa when using elastic moduli in the Hill approximation. Since H_v at 0 GPa is smaller than 10 GPa, both compounds can be classified as relatively soft materials.

Figure 10 shows the pressure evolution of the Vickers hardness with pressure. It is observed that H_v decreases as pressure increases for both oxides. This is related to the fact that the B/G ratio increases with pressure. In this way, both compounds become softer as pressure increases in good agreement with the increase of their ductility (B/G ratio) as stated above. We note that H_v for As_4O_6 decreases notably with pressure approaching 0 GPa at 20 GPa.

Finally, one elastic property which is fundamental for Earth Sciences in order to interpret seismic waves is the average sound velocity, v_m.[51] In polycrystalline materials, v_m is given by[52]

$$v_m = \left[\frac{1}{3}\left(\frac{2}{v_{trans}^3} + \frac{1}{v_{lon}^3}\right)\right]^{-1/3}, \quad (10)$$

where v_{trans} and v_{lon} are the transverse and longitudinal elastic wave velocities of the polycrystalline material which are given by

$$v_{lon} = \left(\frac{B + \frac{4}{3}G}{\rho}\right)^{1/2}, \quad (11)$$

$$v_{trans} = \left(\frac{G}{\rho}\right)^{1/2}, \quad (12)$$

where B and G are the elastic moduli and ρ is the density. Values of the density and wave velocities v_m, v_{lon}, and v_{trans} at 0 GPa are given for both oxides in Table III. Wave

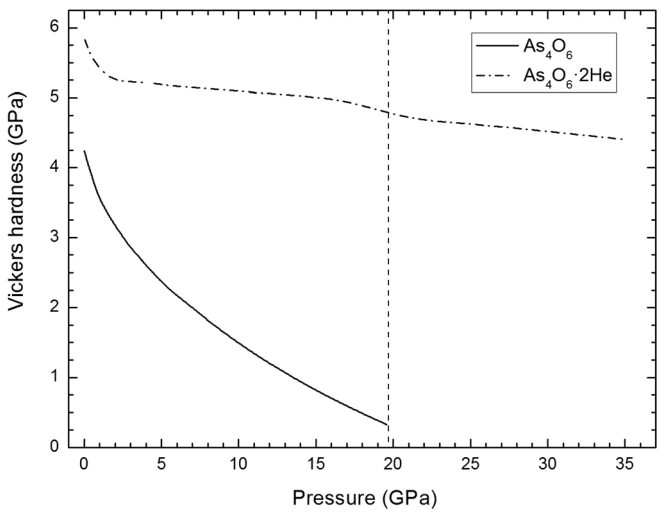

FIG. 10. Evolution with pressure of the Vickers hardness in As_4O_6 and As_4O_6·2He.

velocities are greater for $As_4O_6{\cdot}2He$ than for As_4O_6 because of the higher value of the shear modulus G in the former than in the later and the slightly smaller density of the former than in the later.

Figure 11 reports the evolution with pressure of the elastic wave velocities for both oxides. Using elastic moduli in the Hill approximation, the calculated v_{lon} increases with pressure reaching a value larger than 4725 m/s (5580 m/s) at 20 GPa in As_4O_6 ($As_4O_6{\cdot}2He$). A similar behavior is observed for velocities v_{trans} and v_m in $As_4O_6{\cdot}2He$. However, the corresponding velocities v_{trans} and v_m increase in As_4O_6 reaching a maximum value around 6 GPa and decrease above this pressure.

In order to finish this section, where different magnitudes derived from the elastic constants have been obtained and analysed, we refer the reader to the supplementary material in order to get information on a few thermodynamic properties (Debye temperature and minimum thermal conductivity) obtained for As_4O_6 and $As_4O_6{\cdot}2He$.

D. Mechanical stability

To finish this work, we study the mechanical stability of the cubic structure in As_4O_6 and $As_4O_6{\cdot}2He$ at HP. For that purpose, we make use of the elastic stiffness coefficients reported in Section IV C. The mechanical stability of a crystal at zero pressure can be studied with the Born stability criteria.[53] However, the study of the mechanical stability of a crystal at HP requires the generalization of the Born stability criteria to the case when an external load is applied.[54–56] These generalized stability criteria for cubic crystals with three independent elastic constants are given by the following conditions:

$$M_1 = B_{11} + 2B_{12} > 0, \tag{13}$$

$$M_2 = B_{11} - B_{12} > 0, \tag{14}$$

$$M_3 = B_{44} > 0, \tag{15}$$

where B_{11}, B_{12}, and B_{44} are the elastic stiffness coefficients at the considered pressure. These generalized stability criteria are plotted in Fig. 12 up to 35 GPa. It is found that

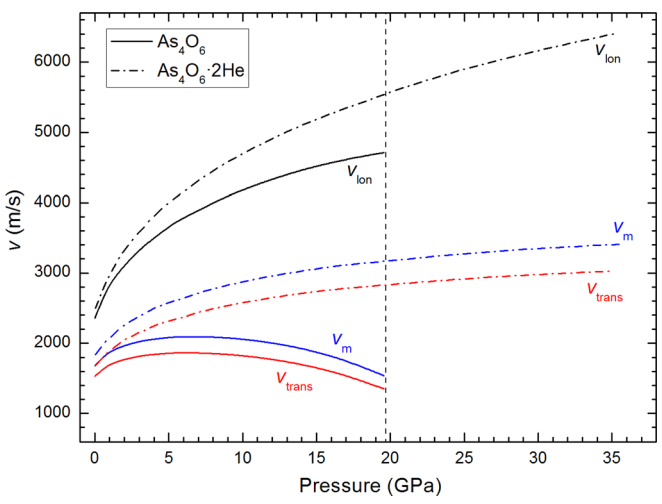

FIG. 11. Pressure dependence of the longitudinal (v_{lon}), transverse (v_{trans}), and average (v_m) elastic wave velocity in As_4O_6 and $As_4O_6{\cdot}2He$.

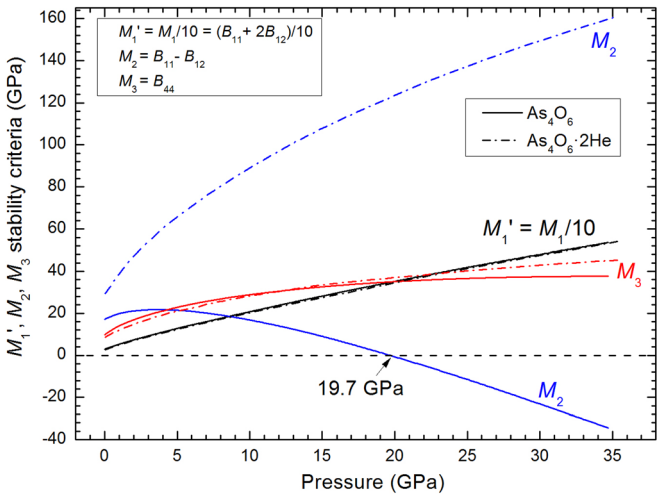

FIG. 12. General stability criteria in As_4O_6 and $As_4O_6{\cdot}2He$. The pressure at which As_4O_6 becomes mechanically unstable is indicated.

Eq. (14), called the Born instability,[55] is violated at 19.7 GPa in As_4O_6; however, none of the three generalized stability criteria is violated in $As_4O_6{\cdot}2He$ up to 35.5 GPa. Therefore, our theoretical study of the mechanical stability suggests that the cubic structure of As_4O_6 becomes mechanically unstable beyond 19.7 GPa, in good agreement with the observation of PIA in the pressure range between 15 and 20 GPa depending on the PTM used.[8,10–12] On the other hand, our calculations show that there is no mechanical instability of $As_4O_6{\cdot}2He$ up to 35.5 GPa, in good agreement with the observation of the cubic phase of this new compound up to 30 GPa.[8,10] Finally, it must be noted that our theoretical results on the mechanical instability of As_4O_6 above 19.7 GPa do not agree with the results on single crystals of As_4O_6 pressurized with He, where He partially entered into the pores of As_4O_6.[9]

V. CONCLUSIONS

We have experimentally and theoretically studied the lattice dynamics of As_4O_6 and $As_4O_6{\cdot}2He$ at HP and found a different HP behavior in the Raman-active modes of both compounds which support the inclusion of He into 16d sites of the arsenolite structure above 2–3 GPa. On the other hand, we have studied the dynamical stability of the cubic structure of both compounds and it has been found that As_4O_6 and $As_4O_6{\cdot}2He$ are dynamically stable at least up to 35 GPa.

Additionally, we have theoretically studied the elastic and thermodynamic behavior of both compounds at HP. It has been found that most of the properties of both compounds are similar at low pressures. The elastic constants and the elastic stiffness coefficients increase with increasing pressure in all the pressure range; however, the pressure coefficients of the elastic stiffness coefficients B_{11} and B_{12} are quite different in both compounds, thus resulting in a completely different HP behavior of shear and Young moduli, B/G ratio, Poisson's ratio, Vickers hardness, and Zener anisotropy in both compounds. In this context, both compounds are more resistive to volume compression than to shear deformation ($B > G$) almost at all pressures. The average elastic wave velocity, Debye temperature, and minimum

thermal conductivity of both compounds are also similar at low pressures but show a different behavior at HP. From the behavior of the elastic stiffness coefficients at HP, we have studied the mechanical stability of the cubic structure at HP in both compounds and have found that the cubic structure becomes mechanically unstable at 19.7 GPa in As_4O_6, while there is no mechanical instability in $As_4O_6{\cdot}2He$ at least up to 35.5 GPa. These results are in good agreement with the experiments which show PIA in As_4O_6 above 15–20 GPa (depending on the PTM used) and with the experimental observation of the cubic structure of $As_4O_6{\cdot}2He$ up to 30 GPa without signs of PIA.

SUPPLEMENTARY MATERIAL

See supplementary material for IR-active modes and thermodynamic properties in As_4O_6 and $As_4O_6{\cdot}2He$ along with the Raman scattering spectra of arsenolite at selected pressures without any PTM.

ACKNOWLEDGMENTS

This study was supported by the Spanish Ministerio de Economía y Competitividad under Projects MAT2013-46649-C4-2-P/3-P, MAT2015-71070-REDC and MAT2016-75586-C4-2-P/4-P. A.M. and P.R.-H. acknowledge computing time provided by Red Española de Supercomputación (RES) and MALTA-Cluster. J.A.S. acknowledges finnancial support from "Ramón y Cajal" fellowship.

[1]S. C. Grund, K. Hanusch, and H. Wolf, "Arsenic and arsenic compounds," in *Ullmann's Encyclopedia of Industrial Chemistry* (Wiley-VCH, 2005).
[2]M. Gielen and E. R. Tiekink, *Metallotherapeutic Drugs and Metal-Based Diagnostic Agents* (John Wiley & Sons, 2005), p. 298.
[3]J. Liu, Y. Lu, Q. Wu, R. A. Goyer, and M. P. Waalkes, J. Pharmacol. Exp. Ther. **326**, 363 (2008).
[4]G. Brauer, *Handbook of Preparative Inorganic Chemistry* (Academic Press, 1963).
[5]G. V. Gibbs, A. F. Wallace, D. F. Cox, P. M. Dove, R. T. Downs, N. L. Ross, and K. M. Rosso, J. Phys. Chem. A **113**, 736 (2009).
[6]P. A. Gunka, Z. Gontarz, and J. Zachara, Phys. Chem. Chem. Phys. **17**, 11020 (2015).
[7]F. Pertlik, Czech. J. Phys. **28**, 170 (1978).
[8]J. A. Sans, F. J. Manjón, C. Popescu, V. P. Cuenca-Gotor, O. Gomis, A. Muñoz, P. Rodríguez-Hernández, J. Pellicer-Porres, A. L. J. Pereira, D. Santamaría-Pérez, and A. Segura, e-print arXiv:1502.04279.
[9]P. A. Gunka, K. F. Dziubek, A. Gladysiak, M. Dranka, J. Piechota, M. Hanfland, A. Katrusiak, and J. Zachara, Cryst. Growth Des. **15**, 3740 (2015).
[10]J. A. Sans, F. J. Manjón, C. Popescu, V. P. Cuenca-Gotor, O. Gomis, A. Muñoz, P. Rodríguez-Hernández, J. Contreras-García, J. Pellicer-Porres, A. L. J. Pereira, D. Santamaría-Pérez, and A. Segura, Phys. Rev. B **93**, 054102 (2016).
[11]A. Grzechnik, J. Solid State Chem. **144**, 416 (1999).
[12]E. Soignard, S. A. Amin, Q. Mei, C. J. Benmore, and J. L. Yarger, Phys. Rev. B **77**, 144113 (2008).
[13]H. K. Mao, J. Xu, and P. M. Bell, J. Geophys. Res. **91**, 4673, doi:10.1029/JB091iB05p04673 (1986).
[14]P. Hohenberg and W. Kohn, Phys. Rev. **136**, B864 (1964).
[15]P. E. Blochl, Phys. Rev. B **50**, 17953 (1994).
[16]G. Kresse and J. Hafner, Phys. Rev. B **47**, 558 (1993); **49**, 14251 (1994); G. Kresse and J. Furthmüller, Comput. Mater. Sci. **6**, 15 (1996); Phys. Rev. B **54**, 11169 (1996).
[17]J. P. Perdew, A. Ruzsinszky, G. I. Csonka, O. A. Vydrow, G. E. Scuseria, L. A. Constantin, X. Zhou, and K. Burke, Phys. Rev. Lett. **100**, 136406 (2008).
[18]K. Parlinski, Z. Q. Li, and Y. Kawazoe, Phys. Rev. Lett. **78**, 4063 (1997).
[19]N. Chetty, A. Muñoz, and R. M. Martin, Phys. Rev. B. **40**, 11934 (1989).
[20]Y. Le Page and P. Saxe, Phys. Rev. B **65**, 104104 (2002).
[21]O. Beckstein, J. E. Klepeis, G. L. W. Hart, and O. Pankratov, Phys. Rev. B **63**, 134112 (2001).
[22]J. F. Nye, *Physical Properties of Crystals. Their Representation by Tensor and Matrices* (Oxford University Press, 1957).
[23]P. Ballirano and A. Maras, Z. Kristallogr. - New Cryst. Struct. **217**, 177 (2002).
[24]E. Kroumova, M. I. Aroyo, J. M. Perez-Mato, A. Kirov, C. Capillas, S. Ivantchev, and H. Wondratschek, Phase Transitions **76**, 155 (2003).
[25]I. R. Beattie, K. M. S. Livingston, G. A. Ozin, and D. J. Reynolds, J. Chem. Soc. A 449 (1970).
[26]J. O. Jensen, S. J. Gilliam, A. Banerjee, D. Zeroka, S. J. Kirkby, and C. N. Merrow, J. Mol. Struct.: THEOCHEM **664–665**, 145 (2003).
[27]H. A. Szymansky, L. Marabella, J. Hoke, and J. Harter, Appl. Spectrosc. **22**, 297 (1968).
[28]S. B. Brumbach and G. M. Rosenblatt, J. Chem. Phys. **56**, 3110 (1972).
[29]D. J. Lockwood, J. Solution Chem. **29**, 1039 (2000).
[30]S. J. Gilliam, C. N. Merrow, S. J. Kirkby, J. O. Jensen, D. Zeroka, and A. Banerjee, J. Solid State Chem. **173**, 54 (2003).
[31]J. A. Sans, F. J. Manjón, C. Popescu, A. Muñoz, P. Rodríguez-Hernández, J. L. Jordá, and F. Rey, J. Phys.: Condens. Matter **28**, 475403 (2016).
[32]M. Born, Proc. Cambridge Philos. Soc. **36**, 160 (1940).
[33]J. D. Clayton, *Nonlinear Mechanics of Crystals*, Solid Mechanics and Its Applications Vol. 177 (Springer, New York, 2010).
[34]D. C. Wallace, "Thermoelastic theory of stressed crystals and higher-order elastic constants," in *Solid State Physics*, edited by F. S. Henry Ehrenreich, D. Turnbull, and F. Seitz (Academic Press, 1970), Vol. 25, pp. 301–404.
[35]J. Wang, S. Yip, S. R. Phillpot, and D. Wolf, Phys. Rev. Lett. **71**, 4182 (1993).
[36]J. Wang, J. Li, S. Yip, S. Phillpot, and D. Wolf, Phys. Rev. B **52**, 12627 (1995).
[37]Z. Zhou and B. Joós, Phys. Rev. B **54**, 3841 (1996).
[38]B. B. Karki, L. Stixrude, and R. M. Wentzcovitch, Rev. Geophys. **39**, 507, doi:10.1029/2000RG000088 (2001).
[39]O. M. Krasil'nikov, M. P. Belov, A. V. Lugovskoy, I. Yu. Mosyagin, and Yu. Kh. Vekilov, Comput. Mater. Sci. **81**, 313 (2014).
[40]W. Voigt, *Lehrbuch der Kristallphysik* (B. G. Teubner, Leipzig, Germany, 1928).
[41]A. Reuss, Z. Angew. Math. Mech. **9**, 49 (1929).
[42]R. Hill, Proc. Phys. Soc., London, Sect. A **65**, 349 (1952).
[43]O. Gomis, D. Santamaría-Pérez, J. Ruiz-Fuertes, J. A. Sans, R. Vilaplana, H. M. Ortiz, B. García-Domene, F. J. Manjón, D. Errandonea, P. Rodríguez-Hernández, A. Muñoz, and M. Mollar, J. Appl. Phys. **116**, 133521 (2014).
[44]R. Caracas and T. B. Ballaran, Phys. Earth Planet. Inter. **181**, 21 (2010).
[45]Q. J. Liu, Z. T. Liu, and L. P. Feng, Commun. Theor. Phys. **56**, 779 (2011).
[46]V. V. Brazhkin, A. G. Lyapin, and R. J. Hemley, Philos. Mag. A **82**, 231 (2002).
[47]G. N. Greaves, A. L. Greer, R. S. Lakes, and T. Rouxel, Nat. Mater. **10**, 823 (2011).
[48]S. F. Pugh, Philos. Mag. **45**, 823 (1954).
[49]V. Tvergaard and J. W. Hutchinson, J. Am. Ceram. Soc. **71**, 157 (1988).
[50]Y. Tian, B. Xu, and Z. Zhao, Int. J. Refract. Met. Hard Mater. **33**, 93 (2012).
[51]J. P. Poirier, *Introduction to the Physics of the Earth's Interior* (Cambridge University Press, 2000).
[52]O. L. Anderson, J. Phys. Chem. Solids **24**, 909 (1963).
[53]M. Born and K. Huang, *Dynamical Theory of Crystal Lattices* (Oxford University Press, 1954), p. 140.
[54]D. C. Wallace, Phys. Rev. **162**, 776 (1967).
[55]G. Grimvall, B. Magyari-Köpe, V. Ozoliņš, and K. A. Persson, Rev. Mod. Phys. **84**, 945 (2012).
[56]H. Wang and M. Li, J. Phys.: Condens. Matter **24**, 245402 (2012).